Can parameterizations reproduce the gravity waves momentum fluxes and drag simulated by a global high resolution model?

I. Toghraei[1], F. Lott[1], L. Köhler[2], C. C. Stephan[3], M. J. Alexander[4]

[1]Laboratoire de Météorologie Dynamique, Institut Pierre-Simon Laplace, PSL Research Institute, Paris, France.
[2]Alfred Wegener Institute, Bremerhaven, Germany.
[3]Department of Modelling of Atmospheric Processes, Leibniz Institute of Atmospheric Physics at the University of Rostock, Kühlungsborn, Germany.
[4]NorthWest Research Associates, Boulder Office, Boulder, CO, USA

keypoints

- Gravity waves (GWs) parameterizations are used to predict the GWs solved in a short range high-resolution global simulation.
- The regions with large GWs activity in the low stratosphere of the global model are quite well captured by the parameterizations.
- An attenuation of the simulated GWs aloft the subtropical jets is described and is underestimated by the parameterization.
- The comparison suggests that the balance between the different sources of GWs should be considered with great care.

Corresponding author: Francois Lott, `francois.lott@lmd.ipsl.fr`

Abstract

We compare the gravity waves (GWs) parameterizations used in the IPSLCM6 climate model to the GWs simulated in the ICON high-resolution global model. The parameterizations are run offline using ICON fields coarse-grained to a 100 km horizontal scale grid and are compared to the GWs momentum fluxes (MFs) and drag due to the smaller scale disturbances and that are resolved in ICON. Overall, the parameterized and resolved drags are comparable and the MFs align well. It also seems that each GWs parameterization (fronts, convection and mountains) plays a role at the right geographical location. Among the differences, we find that in ICON the GWs are substantially attenuated aloft the subtropical jet, this is underestimated by the parameterization. It could be corrected by tuning the characteristic phase speeds or the breaking criteria of the parameterized GWs. The comparison also suggests that ICON underestimates frontal waves.

Plain Language Summary

To simulate the middle atmosphere climate, Earth System Models use parameterizations of small-scale gravity waves that are generated in the troposphere and that propagate and break in the middle atmosphere. The direct in situ observations of these waves are sparse and non-global, their remote satellite observations are more global but still have quite coarse resolutions. To compensate for these deficiencies, the recent high-resolution global simulations of the earth atmosphere are extremely promising because they explicitly solve a good fraction of the gravity wave spectra and their dissipation. Here we show that these simulations are promising to tune existing parameterizations, and in particular adjusting the partition between the different sources of waves or the characteristic phase speeds of the parameterized waves. Reciprocally, these comparisons could help to tell if the global scale high-resolution models produce more or less gravity waves than needed for the middle atmosphere climate.

1 Introduction

Gravity waves (GWs) are generated by various sources, mainly in the troposphere, such as flow over mountains (Lilly & Kennedy, 1973), convection (Fovell et al., 1992), and imbalances in jets and fronts (Plougonven & Zhang, 2014). As GWs propagate vertically, they carry horizontal momentum and affect the large-scale circulation when they break (Dunkerton, 1997; M. Alexander & Rosenlof, 2003; Fritts & Alexander, 2003; McLandress & Shepherd, 2009). Since the horizontal scale of the GWs can be much shorter than the 1^o to 2^o horizontal resolution of the atmospheric general circulation models used in earth system models, they need to be parameterized (M. Alexander et al., 2010). State-of-the-art GW parameterization schemes make quite a distinct treatment between the orographic and non-orographic GWs.

In the orographic GW schemes, quite local and detailed information about the source is explicitly taken into account. Such orographic GW parameterizations have been employed for almost 40 years and have proven to be successful in reducing biases in both the upper (Palmer et al., 1986) and lower troposphere (Lott, 1999; Scinocca & McFarlane, 2000). To a certain extent, they have been validated by dedicated in situ observations during field campaigns (Lott & Miller, 1997; Smith & Kruse, 2018), and high-resolution limited area model simulations, i.e. validations that remain very local in space and time. In the non-orographic GW schemes, the numerical and theoretical complexities of treating large ensemble of waves and of their breaking at a reasonable cost have been a major concern. These inherent difficulties have led to the development of globally spectral schemes (Hines, 1997; Warner & McIntyre, 1999) or to treat the large ensemble of waves with stochastic methods (Lott et al., 2012). In these schemes, the introduction of sources is more recent and not systematic. It is generally believed that these sources are convection (Beres et al., 2005; Song & Chun, 2005; Lott & Guez, 2013a) and fronts in the mid-latitude (Charron & Manzini, 2002; De la Cámara & Lott, 2015) (see also (Richter et al., 2010)). Such non-orographic GW parameterizations have also been successfully introduced to reduce biases in the middle atmosphere (Scinocca, 2003; Song & Chun, 2005; Beres et al., 2005; Orr et al., 2010; Lott & Guez, 2013a; De la Cámara & Lott, 2015; Bushell et al., 2015; Anstey et al., 2016; Serva et al., 2018) and their realism has been largely proven indirectly through their impact on the large-scale circulation.

With the most recent global satellite observations, it becomes possible to gain a global view of the GW fields. However, these techniques only detect the large horizontal-scale GWs and mostly measure temperature fluctuations (Geller et al., 2013a) and the momentum fluxes being computed indirectly using polarization relations (M. J. Alexander et al., 2010; Ern et al., 2014). In order to observe the shorter horizontal scales and to have more direct access to the momentum fluxes, in situ observations are more adapted and the most precise measurements are provided by constant-level long-duration balloons like those made in the Antarctic region during Strateole-Vorcore (Hertzog, 2007) and Concordiasi (Rabier et al., 2010), or in the deep tropics during PreConcordiasi (Jewtoukoff et al., 2013) and Strateole 2 (Haase et al., 2018). These observations have helped improve our understanding and parameterizations of GWs (M. Alexander et al., 2021; Lott et al., 2023). Nevertheless, these observations are mainly regional, limited to the lower stratosphere, and cover relatively short periods of time, which limit the scope of the results obtained (Geller et al., 2013b; Achatz et al., 2024).

To complement these incomplete and global or too local datasets global high-resolution models offer a promising avenue. There are at least three reasons for this. First, in these models, GW fields start to be rather realistic when compared with satellite observations (Stephan et al., 2019), with momentum fluxes matching quite decently with those derived from satellite observations. In this regard, it is important to note that the GW dynamics at work in these models is still not fully understood and GW momentum fluxes remain dependent on the model formulation. Secondly, these models start to tell at which resolution GWs no longer need to be parameterized. In this respect, Polichtchouk et al.

(2023) show that GWs still need to be parameterized in global models with grid-scale near 4 km, with some convergence being reached at around 1 km resolution. If true, such low convergence will make that parameterizations will remain necessary in most climate models for the foreseeable future (Achatz et al., 2024). Third and starting again from the results in Polichtchouk et al. (2023), these simulations give information on the partitioning between the different sources of GWs (orographic or non-orographic), which is crucial when tuning parameterizations in large-scale models. For instance, it is essential to achieve the appropriate balance between orographic and non-orographic GWs when simulating the right climate of the middle atmosphere in both the Northern Hemisphere and the Southern Hemisphere. Similarly, achieving the right balance between convective and frontal waves is crucial when trying to reproduce the mid-latitude dynamics and simulate a quasi-biennial oscillation in the tropics.

Based on the success of the GW parameterization schemes to simulate the right climate, the purpose of this paper is to evaluate momentum fluxes parameterized in climate models by comparing them to those explicitly resolved in a recent state-of-the-art high-resolution model. This comparison is an essential step in bridging the gap between observations, models, and parameterizations to consolidate our understanding of the significance of GWs on climate. It also has practical applications. One application is to determine if high-resolution models produce the right amount of waves by directly comparing parameterizations and resolved waves, rather than relying on simulations with increasing resolution. Another is to assess if the GWs dynamics at work in parameterizations are consistent with the GWs dynamics in high-resolution models. To reach these goals, we use the ICOsahedral Nonhydrostatic Weather and Climate Model (ICON), which is a state-of-the-art high-resolution global model capable of simulating GWs explicitly (Hohenegger et al., 2023). The field from this model are "coarse-grained" at horizontal scales near 1^o to mimic the grid scale of an ESM, the subgrid-scale fluxes being due to motions with scales ranging between the model and the coarse-grain resolution. From the coarse-grained fields of winds, temperature, and precipitation, we run in offline mode the GW parameterizations that are operational in the Institute Paul Simon Laplace Coupled Model version for CMIP6 (IPSLCM6,(Boucher et al., 2020)).

The plan of the paper is as follows: Data and Methods are briefly discussed in section §2. In section §3, the temporal mean and zonal mean GW fluxes by the parameterizations are compared with the zonal momentum fluxes simulated by ICON to comprehensively assess the capabilities of the parameterization schemes across different atmospheric regions and layers. Finally, section §4 illustrates how such comparison can highlight the strengths and weaknesses of the parameterization schemes used in a given model.

2 Data and method

2.1 Simulated Zonal momentum flux

To calculate horizontal momentum fluxes due to GWs with horizontal scales smaller than typical climate model grid scales, we take 3-hourly instantaneous output from a 5 year ICON run with atmosphere-ocean coupling performed within the cycle 3 of the project nextGEMS (Koldunov et al., 2023). The horizontal resolution of the icosahedral grid was R2B9 ($\sim$5 km), but the outputs are immediately remapped to a Hierarchical Equal Area isoLatitude Pixelation (Healpix) grid with resolution parameter $N_{\rm side} = 1024$ corresponding to a horizontal resolution ~ 6.3 km. In the vertical, the model has 90 unequally spaced levels up to of $z = 75$ km. In the following, we only use results up to the top of the stratosphere, $z = 50$ km, the altitudes aloft being in the model sponge layer. In the lower stratosphere at 16 km the vertical resolution is near $\sim$ 700 m and at the stratopause at $z = 50$ km it is near $\sim$ 1.75 km. The model was run without GW parameterizations, and for three weeks between March 20 and April 10 2020, we separated the horizontal wind field at each model level into a divergent and a rotational part. With this so-called Helmholtz decomposition (Lindborg, 2015), we reconstructed the divergent part of the horizontal flow at each level, a technique that largely excludes the vortical terms and leaves us approximately with the GW contribution (Stephan et al., 2022). The divergent wind field was then remapped to a Healpix grid with $N_{\text{side}} = 512$ ($\sim$12.7 km). At this still high-resolution, cross products such as uw were calculated, with u and w being the horizontal and vertical winds, respectively. We then averaged fields and cross products to a coarser Healpix grid with a resolution parameter $N_{\text{side}} = 64$, corresponding to $\sim$100 km horizontal resolution. This mapping allows the calculation of the vertical component of a local Eliasen-Palm flux

$$F^z = \rho\,[u'w'] + \rho f \frac{[v'\theta']}{[\theta]_z}, \tag{1}$$

where [ ] is the average over the $N_{\text{side}} = 64$ Healpix coarse grained gridboxes and $u^{'} = u - [u]$. Note also that for the last term on the right, θ is the potential temperature and f is the Coriolis parameter, and that this term was always negligible compared to the first term on the left. In the following, we call this term the momentum flux. To quantify the contribution of these fluxes to the general circulation, we also evaluate their zonal mean (indicated by overlines) and refer to

$$\overline{F}^z = a\cos\phi\left(-\overline{\rho\,[u'w']} + \overline{\rho f \frac{[v'\theta']}{[\theta]_z}}\right), \tag{2}$$

as the contribution of the subgrid-scale waves to the vertical component of the Eliasen Palm flux, a being the earth radius and ϕ the latitude. When used, and to calculate the subgrid-scale wave drag we always include the meridional flux of zonal momentum from the ICON run and estimate the horizontal component of the Eliasen Palm flux by

$$\overline{F}^\phi = -a\cos\phi\,\overline{\rho\,[u'v']}. \tag{3}$$

Note that such a term is not relevant when evaluating the parameterized momentum fluxes, all the schemes we use do not include lateral propagation.

2.2 Parameterized momentum fluxes

For the parameterizations, we next take the non-orographic GWs scheme due to convection and fronts described in Lott and Guez (2013b) and De la Cámara and Lott (2015) respectively. For the orographic GWs, we take the subgrid-scale orography fields calculated as in Lott and Miller (1997) but for the IPSLCM6 grid, and use the version proposed by Lott (1999). Note that there is no tuning, the setup of the schemes used are those from the CMIP6 version of the Laboratoire de Météorologie Dynamique with ”zoom” atmospheric general circulation model (LMDz6, see Hourdin et al. (2020)). The parameterizations are then run offline for the same 21-day period, from 20 March to 10 April 2020, using the coarse-grained three-dimensional wind, temperature, and precipitation fields of ICON.

3 Results

Figure 1 shows the global distribution of the 21-day averages of the resolved and parameterized momentum fluxes at $z = 8$ km, 16 km, and 23 km (bottom).

In the first row which falls within the troposphere, we recover the results in Wei et al. (2022) or Köhler et al. (2023) and find that the simulated fluxes are much larger than the parameterized ones. As these authors show, this is likely because in the troposphere many diabatically and dynamically forced circulations can produce momentum fluxes unrelated to GWs. To a certain extent, Wei et al. (2022) managed to separate in those fluxes the GW and non-GW contributions by applying filtering criteria based

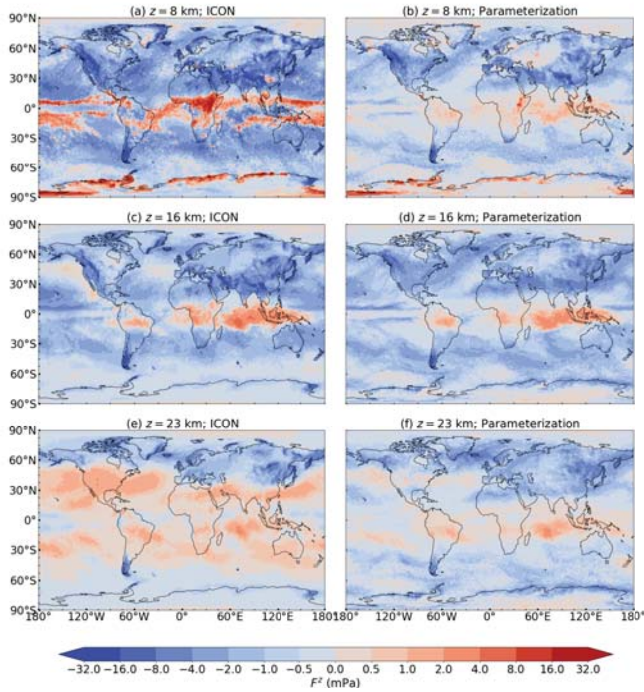

Figure 1. Global distribution of the 21-day mean net zonal momentum fluxes simulated by ICON (left) and predicted by the parameterization schemes using ICON meteorological fields (right) at (a,b) $z = 8$ km, (c,d) $z = 16.4$ km, and (e,f) $z = 22.9$ km.

on precipitation. We attempted a similar approach by selecting coarse-grained grids where precipitations are weak but it did not help much in the context of our direct comparison to parameterizations.

In the lower stratosphere at $z = 16$ km (Figs. 1(c) and 1(d)), the momentum fluxes show better agreement in terms of sign and magnitude. They are quite large and predominantly negative over the mountain ranges in the mid-latitudes. Over the oceans still in the mid-latitudes and subtropics, the net fluxes are also predominantly negative, with the resolved and parameterized fluxes being again of similar amplitude. There are however substantial geographic differences, with a global shift of the parameterized fluxes toward the polar regions over oceans. More precisely, in the southern hemisphere, the resolved fluxes have a band of maximum activity around 30^{o}S (Fig. 1(c)), while it is near 10^o southward in the parameterization (Fig. 1(d)). Furthermore, in the Northern Hemisphere, for instance over the Atlantic Ocean East of Newfoundland to the North East of the Atlantic Ocean (along the storm track), the parameterizations predict quite intense and negative fluxes whereas the resolved fluxes are much less pronounced there.

On the other hand, in the tropics, the locations and signs of the fluxes are quite well predicted. In the eastward Pacific, there are intense negative fluxes over the 2 branches of the ITCZ, and positive fluxes over Brazil, equatorial Africa, the Indian Ocean and the maritime continent. Similar to the predictions over mid-latitude lands and mountains, it seems that the parameterizations are performing well.

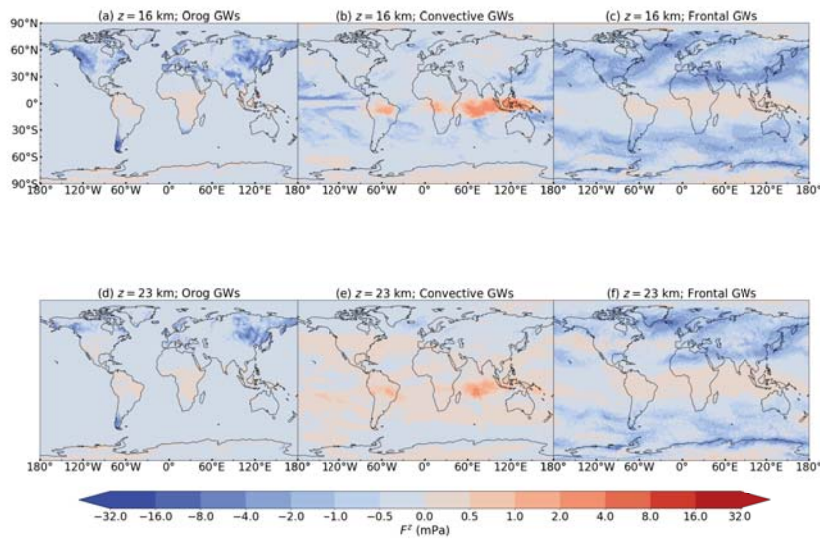

Figure 2. Global distribution of the 21-day mean net zonal parameterized momentum fluxes using ICON meteorological fields: orographic GWs (left), convective GWs (middle), and frontal GWs (right), at $z = 16$ km (first row) and $z = 23$ km (second row).

To understand what causes the similarities and differences between the resolved and parameterized fluxes at 16 km, Fig. 2 shows the contribution of the three GW parameterizations. The better predictions in mid-latitude lands and the tropics mainly result from the orographic GW parameterization and the convective GW parameterization, respectively (Figs. 2(a) and 2(b)). The frontal GW parameterization is also helpful in some sub-tropical regions over the continent (Northern Africa, South Asia and even the Antarctica border). However, it is the main cause of error, leading to excessively large fluxes, for instance, in the mid-latitude storm tracks.

Returning to the comparison between the resolved and parameterized fluxes and analyzing the maps at $z = 23$km in Figs. 1(e) and 1(f), the differences are much more pronounced than at $z = 16$ km. In contrast with the fluxes at $z = 16$ km, simulated net fluxes are of the opposite sign at $z = 23$ km: they are positive almost everywhere in the subtropics and mid-latitudes, they only stay negative in the Northern regions and over land. This change of sign in the subtropics between $z = 16$ km and $z = 23$ km is not observed in the parameterization as show Figs. 1(d), 1(f). There is at least one good reason for this to occur, and it is again illustrated in Fig. 2 showing the net fluxes from the different parameterizations. Figs 2(b) and 2(e) show that the fluxes due to the convective GWs in the subtropics change sign in many places in the subtropics between $z = 16\ km$ and $z = 23\ km$. Such a difference is not seen between the fluxes due to the frontal GW, again because these fluxes are more poleward than the convective GW fluxes.

The results on the time-averaged net fluxes discussed so far hide that in each region, the wave field consists of both negative and positive phase speed waves, which can largely oppose at low altitudes in the stratosphere but result in drags of different signs at different places and altitudes in the middle atmosphere. It is also possible that at a given place and time, predominantly negative phase speed GWs could be hidden by predominantly positive phase speed GWs at another time. Nevertheless and in ICON, it is almost impossible to make such a separation between eastward and westward waves because it necessitates huge storages in the time-horizontal space to make space time Fourier transforms of the subgrid-scale motion. For this reason and to get some insight into the amplitude of the eastward and westward waves separately, an approximation is made assuming that at a given place and time, the GW field is dominated by signed definite phase speed GWs and attribute all the net fluxes of a given sign to GWs with intrinsic phase speed of that sign. We apply this approximation to the parameterized and resolved fluxes to make things comparable.

The temporal average of these sign definite fluxes are shown in Fig. 3. The first important thing to notice is that they have amplitudes comparable with the net fluxes in Fig. 1. It means that in most places, the time average of the net fluxes is not the result of large positive and negative fluxes occurring at different times and canceling each other out. This being noticed, the most remarkable result is that with this east-west separation, the resolved and parameterized fluxes continue to be comparable, with about the same differences as the net fluxes: at $z = 16\ km$ there are too strong parameterized fluxes over oceans in the mid-latitudes, too small parameterized fluxes in the subtropics and about the right amplitude fluxes in the equatorial regions. Importantly also, over the major mountain ranges and mid-latitude lands, the westward fluxes consistently dominate. This is largely due to orographic GWs since momentum fluxes of orographic GWs are mostly negative on the predominantly eastward mid-latitude zonal winds. Finally, and consistent with our interpretation that the westward waves are absorbed in the subtropics between 16 km and 23 km, the resolved westward fluxes are considerably reduced at $z = 23\ km$ compared to $z = 16\ km$, whereas the eastward fluxes are not. To a certain extent, a similar pattern is observed for the parameterized fluxes in the subtropics.

To interpret the difference between the altitudes $z = 16\ km$ and $z = 23\ km$, and to see the impacts on the large-scale circulation of these fluxes, Fig. 4 shows the zonal and temporal mean of the zonal wind in ICON (contour lines) and of the GW drags, calculated from the divergence of the resolved EP flux in ICON,

$$\frac{1}{\rho a \cos\phi}\left(\frac{\partial \cos\phi\,\overline{F}^{\phi}}{\partial\phi} + \frac{\partial \overline{F}^{z}}{\partial z}\right), \qquad (4)$$

in Fig. 4(a) and from the GW parameterizations in Fig. 4(b).

Fig. 4 shows that in the upper troposphere lower stratosphere and aloft the tropospheric jet center (located at around $\pm 40^o$), the zonal mean zonal wind shear is strongly negative between $z = 14\ km$ and $z = 20\ km$. In these regions Fig. 4(a) shows that the GW drag from ICON is negative indicating that significantly more westward GWs break or encounter critical levels than eastward GWs. This is consistent with the theoretical fact that in negative shears, the intrinsic phase speed of westward GWs decreases in amplitude with altitude: these waves saturate at a lower amplitude than the eastward GWs or encounter critical lines as they propagate up. If we now return to the difference between the negative fluxes at $z = 16\ km$ in Fig. 3(e) and at $z = 21\ km$ in Fig. 3(g) one sees that this dynamical filtering of the westward waves occurs around latitudes ± 40 and much more pronounced than for the eastward waves in Figs. 3(a) and 3(c).

If we now analyzed the parameterized values, one sees that the drag Fig. 4(b) is only slightly negative in the northern hemisphere aloft the subtropical jet, the dynamical filtering of the parameterized westward waves seems much less pronounced than for that of the simulated waves. This is in agreement with the maps of positive and negative fluxes in Figs. 3(b), 3(d) and Figs. 3(f), 3(h). Remember nevertheless that in the parameterizations, we found substantial dynamical filtering of the convective waves in the subtropical regions (Figs. 2(b) and 2(e))), confirming that these waves are underrepresented compared to the frontal waves in the parameterizations.

So far, we have established that the parameterizations predict quite realistic fluxes entering the middle atmosphere, but underestimate the attenuation of GWs at the subtropical tropopause. Nevertheless, the simulations and parameterizations can be also compared further aloft where some resemblances are worth noticing. Below the stratopause at $z = 50\ km$ and in the mid-latitude north and south of $\pm 40^o$ respectively, both ICON and the parameterizations present negative drags with comparable amplitudes of a few m/s. What is remarkable here is that the amplitudes somehow compare, and this occurs although GW drags in models are often tuned for acting further aloft in the mesosphere whereas in ICON the drags are produced explicitly. To a certain extent, it tells that the breaking of GWs in the parameterization scheme is quite realistically represented. In both also, the GW drag is negative and large in amplitude where the wind is positive, consistent with the fact that the negative phase speed waves have been dynamically filtered before reaching the upper stratosphere. Analyzing with more details reveals marked differences, for instance, around the polar and mid-latitude regions near below 50 km in the Southern Hemisphere, the parameterized drag is much stronger and negative than the resolved drag. To a certain extent, this is related to the fact that the frontal GWs MF is very large and negative in the northern and mid-latitude in the Southern Hemisphere (see Fig. 2(f) and compare to the resolved momentum flux in Fig. 1(e)). The differences are more pronounced in the Southern Hemisphere than in the Northern Hemisphere, probably because in the Northern Hemisphere too large parameterized frontal waves are equilibrated by smaller orographic drag. Other resemblances and differences can be found in the equatorial and subtropical upper stratosphere (i.e. where $30 < z < 50\ km$), where both the resolved and parameterized drags are consistently positive with maxima where the zonal wind is negative with positive shear. The resolved amplitudes are larger than the parameterized ones (Figs. 4(a),4(b)), to a certain extent this can be related to the fact that the entering net flux at $z = 16\ km$ seems slightly more positive in the subtropical and equatorial regions in Fig. 1(c) than in Fig. 1(d). As show Figs. 1(e) and 1(f) it is more likely related to the dynamical filtering of the westward waves in the subtropics already discussed.

4 Conclusion

This study uses high-resolution simulations done with ICON to estimate the momentum fluxes due to disturbances with horizontal scale below that of a target "coarse-grained" grid of resolution $\approx 100\ km$, somehow representative of the grid of a climate model. These MFs are then predicted by the GW parameterization schemes used in the IPSLCM6 climate model, the input field for the parameterizations being the ICON fields averaged over the "coarse-grained" grid. An important result is that the MFs entering in the middle atmosphere are quite well predicted in amplitude and geographical location. The high resolution model also shows a substantial diminution of the westward propagating waves in the lower stratosphere aloft the subtropical jet that the parameterization underestimates. To a certain extent, this difference is attributed to the fact that the parameterizations overstate the significance of frontal waves compared to convective waves, the latter showing being more dissipated as they are mostly forced in the subtropics. Preliminary tests also show that this underestimation of the gravity wave dissipation in the low stratosphere can be further corrected by imposing smaller intrinsic phase speed waves and/or the parameter that control the amplitude at which the parameterized gravity waves break. The comparison also suggests that in IPSLCM6, the frontal GW parameterization is overestimating the GWs, and to balance this the orographic GWs are underestimated. The parameterizations also make reasonable predictions of the zonal mean GW drag in the stratosphere with some positive drag missing near the subtropical stratopause, may be a result of the lack of dynamical filtering of the westward waves discussed before.

The resemblances and differences we find here are certainly model and parameterizations dependent. This is a deliberate choice: the parameterization schemes used have not been tuned before the comparison, and the middle atmosphere climatology of ICON has not yet been thoroughly tested. Also, we know that these high-resolution simulations have not yet converged when it comes to GWs simulation (Polichtchouk et al., 2023), and that the GWs signal in them is very sensitive to the model formulation (Stephan et al., 2022). This being said, our study illustrates the potential for high-resolution simulations to be used to improve parameterizations, for instance, the balance to be found between the different sources of waves (orographic versus non-orographic, and may be convective versus fronts). Within a given scheme, it also suggests which parameters could be changed to gain realism. In return, our results can also serve as a guidance to tell if high resolution models predict the right amount of waves. After all, the parameterizations have been tuned to reproduce a right climate in the middle atmosphere, this is an indirect evidence of their realism. As an illustration, we have seen that our frontal waves parameterizations predict to large momentum fluxes, but it can also be that in ICON, the resolved waves over fronts are underestimated, simply because its horizontal resolution is still too coarse to resolve well the geostrophic adjustments. We can also imagine that with increasing horizontal resolution the global models overestimate the GWs signal, for instance, because there remain too dissipative at the smaller scales staying too much in a linear regime that favors GWs dynamics. In this case, the GW drags predicted by the parameterizations become an important upper bound to validate the high resolution models. Therefore and to appreciate the mutual benefits, it will be interesting in the future to tune the GW parameterizations to improve their fit with high-resolution simulations systematically and to test in return if this is beneficial to the climate models.

Data availability statement

All data and routines needed to run the parameterizations in offline mode and to compare the results with the coarse grain ICON fields can be downloaded from Zenodo (Toghraei, 2024).

Acknowledgments

This work was supported by the VESRI Schmidt Future project ”Datawave”.

References

Achatz, U., Alexander, M., Becker, E., Chun, H.-Y., Dörnbrack, A., Holt, L., ... others (2024). Atmospheric gravity waves: Processes and parameterization. *Journal of the Atmospheric Sciences*, *81*(2), 237–262.

Alexander, M., Geller, M., McLandress, C., Polavarapu, S., Preusse, P., Sassi, F., ... others (2010). Recent developments in gravity-wave effects in climate models and the global distribution of gravity-wave momentum flux from observations and models. *Quarterly Journal of the Royal Meteorological Society*, *136*(650), 1103–1124.

Alexander, M., Liu, C., Bacmeister, J., Bramberger, M., Hertzog, A., & Richter, J. (2021). Observational validation of parameterized gravity waves from tropical convection in the whole atmosphere community climate model. *Journal of Geophysical Research: Atmospheres*, *126*(7), e2020JD033954.

Alexander, M., & Rosenlof, K. H. (2003). Gravity-wave forcing in the stratosphere: Observational constraints from the upper atmosphere research satellite and implications for parameterization in global models. *Journal of Geophysical Research: Atmospheres*, *108*(D19).

Alexander, M. J., Geller, M., McLandress, C., Polavarapu, S., Preusse, P., Sassi, F., … Watanabe, S. (2010). Recent developments in gravity-wave effects in climate models and the global distribution of gravity-wave momentum flux from observations and models. *Q. J. R. Meteorol. Soc.*, *136*, 1103-1124. doi: https://doi.org/10.1002/qj.637

Anstey, J. A., Scinocca, J. F., & Keller, M. (2016). Simulating the qbo in an atmospheric general circulation model: Sensitivity to resolved and parameterized forcing. *Journal of the Atmospheric Sciences*, *73*(4), 1649 - 1665. doi: https://doi.org/10.1175/JAS-D-15-0099.1

Beres, J. H., Garcia, R. R., Boville, B. A., & Sassi, F. (2005). Implementation of a gravity wave source spectrum parameterization dependent on the properties of convection in the whole atmosphere community climate model (waccm). *Journal of Geophysical Research: Atmospheres*, *110*(D10). doi: https://doi.org/10.1029/2004JD005504

Boucher, O., Servonnat, J., Albright, A. L., Aumont, O., Balkanski, Y., Bastrikov, V., … Vuichard, N. (2020). Presentation and evaluation of the ipsl-cm6a-lr climate model. *Journal of Advances in Modeling Earth Systems*, *12*(7), e2019MS002010. doi: https://doi.org/10.1029/2019MS002010

Bushell, A. C., Butchart, N., Derbyshire, S. H., Jackson, D. R., Shutts, G. J., Vosper, S. B., & Webster, S. (2015). Parameterized gravity wave momentum fluxes from sources related to convection and large-scale precipitation processes in a global atmosphere model. *Journal of the Atmospheric Sciences*, *72*(11), 4349–4371. doi: https://doi.org/10.1175/JAS-D-15-0022.1

Charron, M., & Manzini, E. (2002). Gravity waves from fronts: Parameterization and middle atmosphere response in a general circulation model. *Journal of the Atmospheric Sciences*, *59*(5), 923 - 941. doi: 10.1175/1520-0469(2002)059⟨0923:GWFFPA⟩2.0.CO;2

De la Cámara, A., & Lott, F. (2015). A parameterization of gravity waves emitted by fronts and jets. *Geophysical Research Letters*, *42*(6), 2071–2078.

Dunkerton, T. J. (1997). The role of gravity waves in the quasi-biennial oscillation. *Journal of Geophysical Research: Atmospheres*, *102*(D22), 26053–26076.

Ern, M., Ploeger, F., Preusse, P., Gille, J., Gray, L. J., Kalisch, S., … Riese, M. (2014). Interaction of gravity waves with the QBO: A satellite perspective. *Journal of Geophysical Research: Atmospheres*, *119*, 2329 - 2355. doi: https://doi.org/10.1002/2013JD020731

Fovell, R., Durran, D., & Holton, J. (1992). Numerical simulations of convectively generated stratospheric gravity waves. *Journal of Atmospheric Sciences*, *49*(16), 1427–1442.

Fritts, D. C., & Alexander, M. (2003). Gravity wave dynamics and effects in the middle atmosphere. *Reviews of geophysics*, *41*(1).

Geller, M. A., Alexander, M., Love, P. T., Bacmeister, J., Ern, M., Hertzog, A., … others (2013b). A comparison between gravity wave momentum fluxes in observations and climate models. *Journal of Climate*, *26*(17), 6383–6405.

Geller, M. A., Alexander, M. J., Love, P. T., Bacmeister, J., Ern, M., Hertzog, A., … Zhou, T. (2013a). A comparison between gravity wave momentum fluxes

in observations and climate models. *J. Atmos. Sci.*, *26*(17).
Haase, J. S., Alexander, M. J., Hertzog, A., Kalnajs, L. E., Deshler, T., Davis, S. M., ... Venel, S. (2018). Around the world in 84 days [Dataset]. *Eos*, *99*. doi: https://doi.org/10.1029/2018EO091907
Hertzog, A. (2007). The stratéole-vorcore long-duration balloon experiment: A personal perspective. *Space Research Today*, *169*, 43-48. doi: https://doi.org/10.1016/S1752-9298(07)80047-8
Hines, C. O. (1997). Doppler-spread parameterization of gravity-wave momentum deposition in the middle atmosphere. part 2: Broad and quasi monochromatic spectra, and implementation. *J. Atmos. Solar Terr. Phys.*, *59*(4), 387-400. doi: 10.1016/S1364-6826(96)00080-6
Hohenegger, C., Korn, P., Linardakis, L., Redler, R., Schnur, R., Adamidis, P., ... others (2023). Icon-sapphire: simulating the components of the earth system and their interactions at kilometer and subkilometer scales. *Geoscientific Model Development*, *16*(2), 779–811.
Hourdin, F., Rio, C., Grandpeix, J.-Y., Madeleine, J.-B., Cheruy, F., Rochetin, N., ... others (2020). Lmdz6a: The atmospheric component of the ipsl climate model with improved and better tuned physics. *Journal of Advances in Modeling Earth Systems*, *12*(7), e2019MS001892.
Jewtoukoff, V., Plougonven, R., & Hertzog, A. (2013). Gravity waves generated by deep tropical convection: Estimates from balloon observations and mesoscale simulations. *Journal of Geophysical Research: Atmospheres*, *118*(17), 9690-9707. doi: https://doi.org/10.1002/jgrd.50781
Koldunov, N., Kölling, T., Pedruzo-Bagazgoitia, X., Rackow, T., Redler, R., Sidorenko, D., ... Ziemen, F. A. (2023). *nextgems: output of the model development cycle 3 simulations for icon and ifs.* World Data Center for Climate (WDCC) at DKRZ. doi: 10.26050/WDCC/nextGEMS_cyc3
Köhler, L., Green, B., & Stephan, C. C. (2023). Comparing loon superpressure balloon observations of gravity waves in the tropics with global storm-resolving models. *Journal of Geophysical Research: Atmospheres*, *128*(15), e2023JD038549. doi: https://doi.org/10.1029/2023JD038549
Lilly, D., & Kennedy, P. (1973). Observations of a stationary mountain wave and its associated momentum flux and energy dissipation. *Journal of Atmospheric Sciences*, *30*(6), 1135–1152.
Lindborg, E. (2015). A helmholtz decomposition of structure functions and spectra calculated from aircraft data. *Journal of Fluid Mechanics*, *762*, R4. doi: 10.1017/jfm.2014.685
Lott, F. (1999). Alleviation of stationary biases in a GCM through a mountain drag parameterization scheme and a simple representation of mountain lift forces. *Monthly Weather Review*, *127*(5), 788 - 801. doi: 10.1175/1520-0493(1999)127⟨0788:AOSBIA⟩2.0.CO;2
Lott, F., & Guez, L. (2013a). A stochastic parameterization of the gravity waves due to convection and its impact on the equatorial stratosphere. *J. Geophys. Res.*, *118*(16), 8897-8909. doi: 10.1002/jgrd.50705
Lott, F., & Guez, L. (2013b). A stochastic parameterization of the gravity waves due to convection and its impact on the equatorial stratosphere. *Journal of Geophysical Research: Atmospheres*, *118*(16), 8897–8909.
Lott, F., Guez, L., & Maury, P. (2012). A stochastic parameterization of non-orographic gravity waves: Formalism and impact on the equatorial stratosphere. *Geophys. Res. Lett.*, *39*(6), L06807. doi: 10.1029/2012GL051001
Lott, F., & Miller, M. J. (1997). A new subgrid-scale orographic drag parametrization: Its formulation and testing. *Quarterly Journal of the Royal Meteorological Society*, *123*(537), 101–127.
Lott, F., Rani, R., Podglajen, A., Codron, F., Guez, L., Hertzog, A., & Plougonven, R. (2023). Direct comparison between a non-orographic gravity wave drag

scheme and constant level balloons. *Journal of Geophysical Research: Atmospheres*, *128*(4), e2022JD037585.

McLandress, C., & Shepherd, T. G. (2009). Simulated anthropogenic changes in the brewer–dobson circulation, including its extension to high latitudes. *Journal of Climate*, *22*(6), 1516–1540.

Orr, A., Bechtold, P., Scinocca, J., Ern, M., & Janiskova, M. (2010). Improved middle atmosphere climate and forecasts in the ecmwf model through a nonorographic gravity wave drag parameterization. *Journal of Climate*, *23*(22), 5905 - 5926. doi: https://doi.org/10.1175/2010JCLI3490.1

Palmer, T. N., Shutts, G. J., & Swinbank, R. (1986). Alleviation of a systematic westerly bias in general circulation and numerical weather prediction models through an orographic gravity wave drag parametrization. *Quarterly Journal of the Royal Meteorological Society*, *112*(474), 1001-1039. doi: 10.1002/qj.49711247406

Plougonven, R., & Zhang, F. (2014). Internal gravity waves from atmospheric jets and fronts. *Reviews of Geophysics*, *52*(1), 33–76.

Polichtchouk, I., Van Niekerk, A., & Wedi, N. (2023). Resolved gravity waves in the extratropical stratosphere: Effect of horizontal resolution increase from o (10) to o (1) km. *Journal of the Atmospheric Sciences*, *80*(2), 473–486.

Rabier, F., Bouchard, A., Brun, E., Doerenbecher, A., Guedj, S., Guidard, V., … Steinle, P. (2010, January). The Concordiasi Project in Antarctica. *Bulletin of the American Meteorological Society*, *91*(1), 69-86. doi: 10.1175/2009BAMS2764.1

Richter, J. H., Sassi, F., & Garcia, R. R. (2010). Toward a physically based gravity wave source parameterization in a general circulation model. *Journal of the Atmospheric Sciences*, *67*(1), 136 - 156. doi: 10.1175/2009JAS3112.1

Scinocca, J. F. (2003). An accurate spectral nonorographic gravity wave drag parameterization for general circulation models. *Journal of the Atmospheric Sciences*, *60*(4), 667 - 682. doi: https://doi.org/10.1175/1520-0469(2003)060⟨0667:AASNGW⟩2.0.CO;2

Scinocca, J. F., & McFarlane, N. A. (2000). The parametrization of drag induced by stratified flow over anisotropic orography. *Quarterly Journal of the Royal Meteorological Society*, *126*(568), 2353-2393. doi: https://doi.org/10.1002/qj.49712656802

Serva, F., Cagnazzo, C., Riccio, A., & Manzini, E. (2018). Impact of a stochastic nonorographic gravity wave parameterization on the stratospheric dynamics of a general circulation model. *Journal of Advances in Modeling Earth Systems*, *10*(9), 2147-2162. doi: https://doi.org/10.1029/2018MS001297

Smith, R. B., & Kruse, C. G. (2018). A gravity wave drag matrix for complex terrain. *Journal of the Atmospheric Sciences*, *75*(8), 2599 - 2613. doi: 10.1175/JAS-D-17-0380.1

Song, I.-S., & Chun, H.-Y. (2005). Momentum flux spectrum of convectively forced internal gravity waves and its application to gravity wave drag parameterization. part i: Theory. *J. Atmos. Sci.*, *62*(1), 107-124. doi: https://doi.org/10.1175/JAS-3363.1

Stephan, C. C., Duras, J., Harris, L., Klocke, D., Putman, W. M., Taylor, M., … Ziemen, F. (2022). Atmospheric energy spectra in global kilometre-scale models. *Tellus A: Dynamic Meteorology and Oceanography*(74(1)), 280-299. doi: 10.16993/tellusa.26

Stephan, C. C., Strube, C., Klocke, D., Ern, M., Hoffmann, L., Preusse, P., & Schmidt, H. (2019). Gravity waves in global high-resolution simulations with explicit and parameterized convection. *Journal of Geophysical Research: Atmospheres*, *124*(8), 4446–4459.

Toghraei, I. (2024). *Icon data for spring 2020: March 20 to april 10 release (version 1.0.0).* Zenodo. Retrieved from `https://doi.org/10.5281/zenodo.13946360`

([Code and data files]) doi: 10.5281/zenodo.13946360
Warner, C. D., & McIntyre, M. E. (1999). Toward an ultra-simple spectral gravity wave parameterization for general circulation models. *Earth, Planets and Space*, *51*, 475–484. doi: 10.1186/BF03353209
Wei, J., Zhang, F., Richter, J. H., Alexander, M., & Sun, Y. Q. (2022). Global distributions of tropospheric and stratospheric gravity wave momentum fluxes resolved by the 9-km ecmwf experiments. *Journal of the Atmospheric Sciences*, *79*(10), 2621–2644.

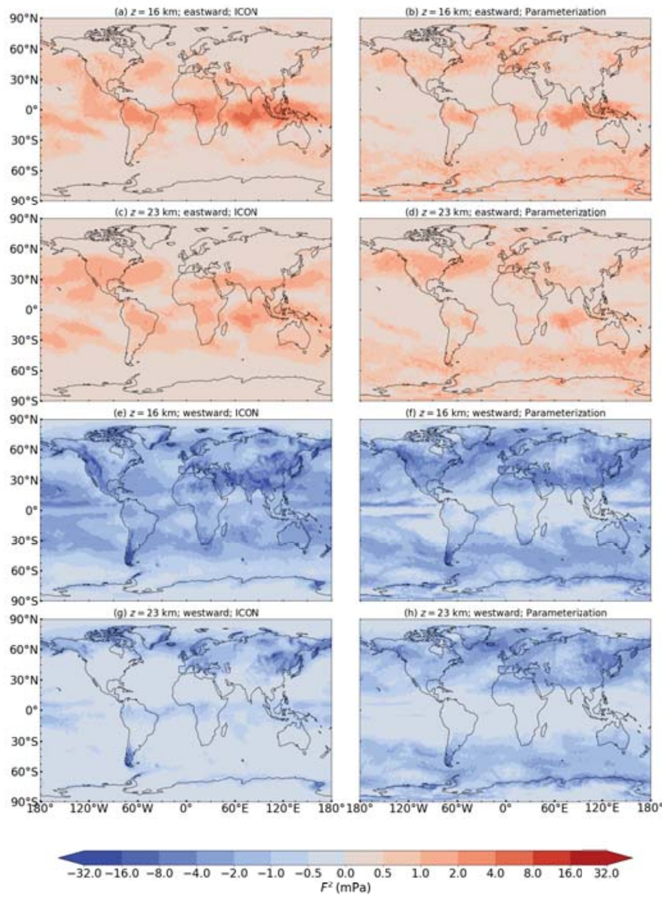

Figure 3. Global distribution of the 21-day mean of the "sign definite" positive and negative zonal momentum fluxes simulated by ICON (left) and predicted by the parameterization schemes (right). The eastward fluxes are in the top four panels, the westward in the bottom four panels. The altitude $z = 16$ km in (a,b,e,f) and $z = 23$ km in (c,d,g,h).

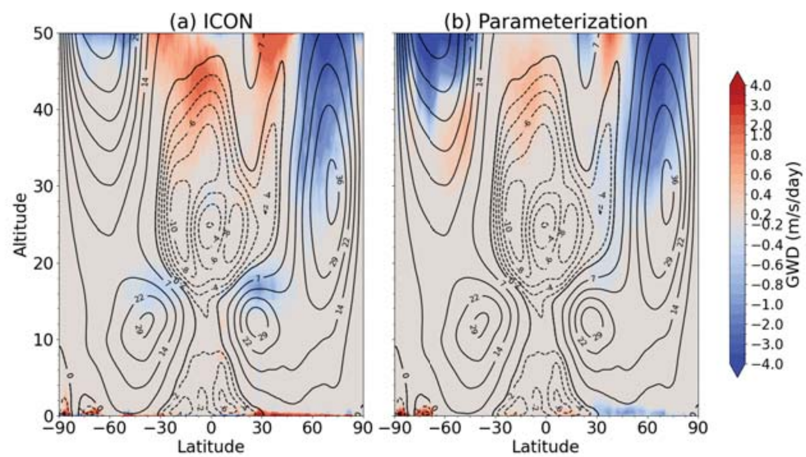

Figure 4. Zonal mean 21-day mean of the resolved (a) and parameterized (b) GW drag. Solid and dashed contour lines represent eastward and westward of the zonal mean 21-day mean zonal wind, respectively.